Flame-Assisted Spray Pyrolysis Using an Annular Flame Nozzle with Decoupled Velocity Control

Maxym Rukosuyev, Syed Baqar, Jungsoo Nam, Huitaek Yun and Martin Byung-Guk Jun

October 2018

Journal of
Manufacturing and Materials Processing

MDPI

Article

Flame-Assisted Spray Pyrolysis Using an Annular Flame Nozzle with Decoupled Velocity Control

Maxym Rukosuyev [1], Syed Baqar [1], Jungsoo Nam [2], Huitaek Yun [3] and Martin Byung-Guk Jun [3,*]

[1] Department of Mechanical Engineering, University of Victoria, Victoria, BC V8W 2Y2, Canada; maxr@uvic.ca (M.R.); alib@uvic.ca (S.B.)
[2] Department of Manufacturing System R&D, Korea Institute of Industrial Technology, Cheonan 31056, Korea; rack1219@kitech.re.kr
[3] School of Mechanical Engineering, Purdue University, West Lafayette, IN 47906, USA; yun37@purdue.edu
* Correspondence: mbgjun@purdue.edu; Tel.: +1-765-494-3376

Received: 2 August 2018; Accepted: 29 October 2018; Published: 30 October 2018

Abstract: Flame spray pyrolysis, widely used in chemical industries, is a technology to synthesize nanoparticles. While the flame spray pyrolysis uses fuels as a solution liquid, the flame-assisted spray pyrolysis method uses aqueous solutions. Since process parameters such as concentration of precursor, size of droplets, and ratio of the air–gas mixture affect the size of nanoparticles, developing a flexible system to control these parameters is required. This paper proposes a new type of nozzle system to produce nanoparticles using flame-assisted spray pyrolysis. The annular nozzle design allows flexible control of particle flow and temperature, and an ultrasonic nebulizer was used to produce droplets with different size. Experiments were conducted to analyze the relationship between nanoparticle size and process parameters, concentration of precursor, frequency of the atomizer, and flame temperature. A precursor solution consisting of silver nitrate ($AgNO_3$) mixed in deionized water is used. The effects of the process parameters are discussed, and analysis of the nanoparticles shows that silver nanoparticles are deposited with an average size of 25~115 nm.

Keywords: flame-assisted spray pyrolysis; Ag nanoparticles; thermal decomposition

1. Introduction

Flame Spray Pyrolysis is an economic, single-step, and versatile process to synthesize nanosized metals, alloys, and ceramics compared to other technologies such as vapor deposition, laser ablation, and plasma synthesis [1]. A wide range of produced materials are reported in the literature, such as tin dioxide for sensors in semiconductor industry [2], bimetallic materials [3], nanotubes [4], and so on. It is also a single step process, so that subsequent annealing processes are not required other than conventional methods [2]. Due to its single step process characteristic, the method is also applied to roll-to-roll deposition of nanoparticles [5,6].

Spray pyrolysis systems consist of a small droplet generator from precursor solution, a droplet carrier, a high-temperature treatment unit, and a particle collector. An ultrasonic atomizer, one of the droplet generators, produces equally sized droplets, and their flow rate is controlled by a carrier gas. The equation to estimate average droplet diameter is described below [7]:

$$D_P = 0.34\left(\frac{8\pi\sigma}{\rho f^2}\right)^{\frac{1}{3}} \quad (1)$$

where Dp is the diameter of droplets, σ is the surface tension of liquid, ρ is the density of liquid, and f is the atomizer's frequency. From Equation (1), the droplet size varies with parameters of atomizing

transducers, such as supplying power and resonant frequency. For the high-temperature treatment unit, there are several types such as flame reactor and quenching device [8–10], heating substrates [11], diffusion flames from a mixture of a fuel, an oxidant, and a precursor aerosol [12], and spray flames by ignition of the mixture of a fuel and a precursor [13]. The generation and following deposition of nanoparticles varies with the type of treatment unit. Furthermore, when flame spray pyrolysis is used to deposit thin films, a substrate which is usually made of a poly-tetrafluoroethylene (PTFE) or a glass fiber-based filter is placed as an alternative to a particle collection unit [14].

However, the mechanism of how nanoparticles are formed and deposited is not generally defined. Since the process has a number of parameters with various precursors and reactor designs, several researchers [15–17] admitted that the method is not clearly generalized. Pratsinis [16] mentioned that bulk material properties change on the nanoscale because the principle of continuum does not fit to nanoparticles, and therefore the process was verified by experimental results and simulations.

The process parameters and the precursors decide the formation of nanoparticles. Several studies [18–24] have analyzed the effect of different precursors on the formation of nanoparticles. In the study of Cho et al. [18] about producing silica nanoparticles from silicic acid and tetraethyl orthosilicate (TEOS), the formation of particles can be explained by one of three routes: Vapor Phase Reaction (VPR), Intra Droplet Reaction (IDR), and the mixture of two routes. The routes are classified according to spray pyrolysis parameters, especially flame temperature. In case of VPR, the reaction is finished in a vapor phase. This case happens when the time for the precursor droplet to be evaporated is shorter than the time to form nanoparticles, while each duration is decided by flame temperature, precursor concentration, and so on. VPR happens more frequently at low precursor concentration and high flame temperature. Particles start to form aggregates after nucleation and they are deposited onto the substrate. In contrast, in the IDR case, the time taken for precursor droplets to evaporate is longer than that of particle formation. Therefore, precipitation makes tiny seed particles in the precursor droplet. By condensation, seed particles become larger, and precursor droplets are evaporated. In this case, precursors are highly concentrated due to the lower flame temperature than in the VPR case. When VPR and IDR are mixed, the time of precursor evaporation and the one of particle formation are similar, so that both cases are applicable. This explanation gives us understanding of how nanoparticles are formed, although it may not be generalized for all precursors.

It has been known that several parameters affect the shape of nanoparticles. For example, increasing the feed rate of nozzle reduces the amount of precursor per unit area, and fewer particles are deposited. When a mixture of precursor with high flow rate is combined with a carrier gas, shorter duration of particles on the substrate causes less deposition. When the flow rate of the carrier gas is increased, the concentration of precursor droplets and the flame temperature are reduced, resulting smaller particle size [20,25]. The distance between the nozzle end and the substrate decreases the number of deposited particles on the substrate since diffusion and thermophoresis happen at the passage of mixture in the air, decreasing the gradients of particles [5].

Temperatures at the passage and the substrate affect the thickness of the resultant coating. A dense film is formed when the temperature of the substrate is increased by the flame or external sources [2]. Because the flame is from a fuel such as hydrogen, methane, or propane, with oxygen, the flame temperature is decided by a stoichiometric ratio of the fuel and the oxidant. The temperature of hydrogen-air flame reaches up to 2200 °C, but it can be lowered with a lower stoichiometric ratio. A higher flame temperature causes shorter evaporation time and causes formation of smaller particles, but excessive temperature forms aggregates [20]. In addition to the ratio of a fuel to an oxidant, the type of fuel affects the contents of impurities on a film. For example, acetylene at higher temperature generates carbide impurities [26].

While flame spray pyrolysis can hold the flame, since its solution is based on fuels, the modified process called “flame-assisted spray pyrolysis” usually uses aqueous solutions so that they cannot

sustain an initial flame [27,28]. Among particles for flame-assisted spray pyrolysis, silver nitrate ($AgNO_3$) produces silver particles by thermal decomposition:

$$2AgNO_3\ (s) \rightarrow 2Ag\ (s) + O_2\ (g) + 2NO_2\ (g) \quad (2)$$

Plyum et al. [29] produced micron-sized silver nanoparticles from the process. Similarly, other researchers [30,31] created nanoscale particles from a tube furnace and flame spray pyrolysis. Although silver nitrate can be decomposed at relatively low temperature with less energy consumption [32], flame-assisted spray pyrolysis is another method of silver nanoparticle decomposition which provides additional thermal treatment and is applicable to other nanoparticles. However, since the process parameters mentioned above affect the size of the produced nanoparticles, the spray pyrolysis system should flexibly change the parameters.

This paper proposes a new nozzle design to produce nanoparticles and deposit them on a substrate using flame-assisted spray pyrolysis. In Section 2, the nozzle design is introduced to allow flexible adjustment of process parameters. In addition, experimental setups are described to investigate the effects of parameters such as the atomizer's natural frequency, precursor concentration, and flame temperatures on the size of the nanoparticles. In Section 3, studies of the parameters and analysis of deposited nanoparticles are discussed.

2. Nozzle Design and Testing

The structure of a dual velocity deposition nozzle is described in [33], and a port for fuel gas input was added to the literature's nozzle design (Figure 1) so that it can be used for flame spray pyrolysis.

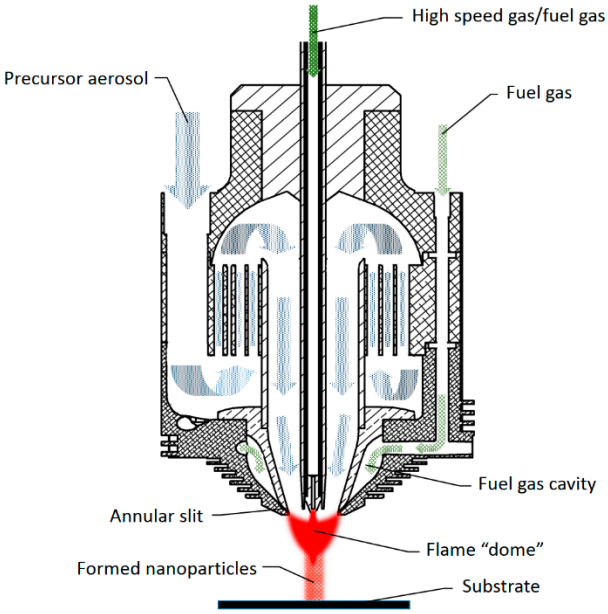

Figure 1. A new nozzle design based on the dual velocity nozzle with an additional fuel injection port.

At the nozzle exit, there is a fuel gas cavity between the inner funnel and outer wall, which forms a narrow annular slit. For the fuel gas, hydrogen is supplied to the circular slit where it is mixed with air (oxidant) at the end of the annular slit. The high-speed oxidizer gas and carrier gas are supplied through a double-walled tube in the center, and the carrier gas controls temperature at the exit. A precursor aerosol is provided from two sides, while only one of the sides is shown in Figure 1. The cyclone effect generates circular motion in the lower section, and large droplets remain on the wall of the lower chamber. The honeycomb structure reduces turbulence of the aerosol, generating nearly axisymmetric flow. The velocity of the aerosol is maintained between 6 m/s and 10 m/s. At

the exit of the nozzle, static pressure in the middle is lowered due to the high velocity of gases at the center. After a dome-shaped flame is formed, the decomposition of precursor and following formation of nanoparticles occur, which are deposited on the substrate or gathered for other uses. Axisymmetric gas flow helps uniform deposition, thereby enabling precise thickness control of a coating layer. In addition, supplying the precursor as an aerosol form allows one to suspend the current precursor and provide a new type of precursor, enabling composite coating.

A schematic of the entire system is described in Figure 2. The ratio of fuel gas to air is finely controlled by separated valves to maintain the optimal temperature for decomposition. Mass flow meters (HFM-200, Teledyne Hastings, Hampton, VA, USA) are installed on the pipes to monitor the flow rate of the gases.

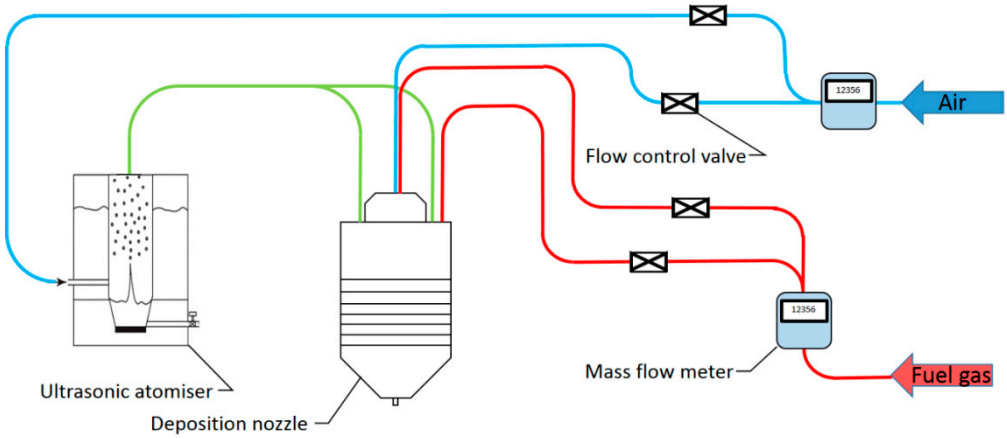

Figure 2. A schematic of the nanoparticle coating system based on flame-assisted spray pyrolysis.

Figure 3 shows the nozzle attached on the CNC router (HS-1, Romaxx CNC Inc., Redford, MI, USA) to control overlap, feed rate, and distance between the nozzle end and the substrate. The power of ultrasonic atomizing transducer was set to 12 W, flow rate was set up to 400 mL/h, and two resonant frequencies (2.4 and 3 MHz) are used. However, the actual flow rate after the atomizer is adjusted by the flow rate of carrier gas.

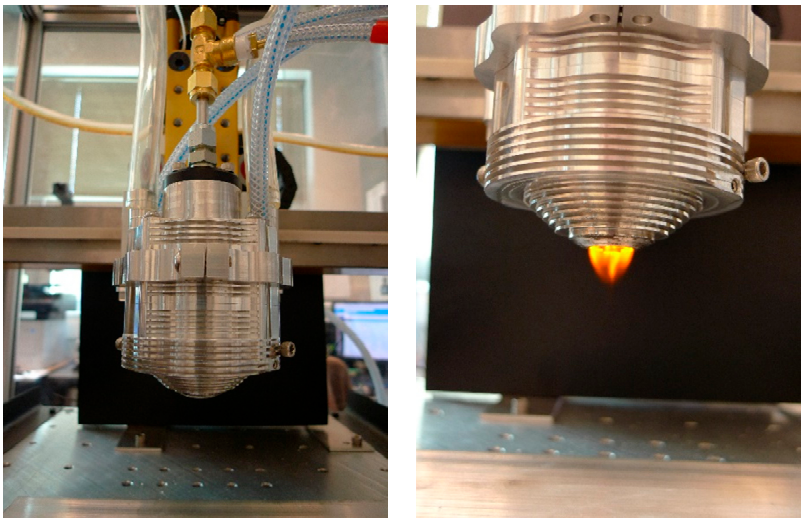

Figure 3. The nozzle system mounted on a CNC router and generated flame.

Experiments were performed to verify the system's capability to deposit nanoparticles on a substrate. To prepare a precursor solution, 250 mg of silver nitrate (250 mg, $AgNO_3$ > 99%, Sigma Aldrich, St. Louis, MO, USA) was dissolved into 250 mL of deionized water, and the solution was mixed

by magnetic stirring for 25 min. According to the literature [34], silver nitrate begins to decompose at 450 °C, and finishes at 520 °C with 63.5% of the mass remained while the residual component is silver. Because $AgNO_3$ reacts to light and produces silver ions, the precursor solution was prepared under low light conditions and the system components were covered with aluminum foil. As for the substrate, an ultra-high vacuum and contamination free aluminum foil (All–Foils Inc. Strongsville, OH, USA) was pasted on an aluminum stub and glued with conductive graphite paste (PELCO Conductive Graphite, Isopropanol base, Ted Pella Inc. Redding, CA, USA). The surface was pre-treated with a corona treater (BD-20, Electro-technics, Chicago, IL, USA) before the deposition to increase the surface energy, thereby stimulating the bonding and adhesion of the surface. The coating was processed with 1.83 m/min feed rate at 22 mm distance between the nozzle tip and the substrate. The nozzle's trajectory was a zigzag style on the surface area of about 6.45 cm^2.

In the first experiment, precursor solutions with three different concentrations (50 mg/L, 100 mg/L, and 200 mg/L) and two resonant frequencies of the ultrasonic atomizer (2.4 MHz and 3 MHz) were tested to observe effects of precursor concentration and droplet size. The experimental setup is summarized in Table 1. Two K-type thermocouples are used to check the desired flame temperature. Each K-type thermocouple was enclosed in a probing structure made of a steel tube of approximately 2.5 mm diameter. The probe was then placed into the corresponding position for thermal measurements using a bracket. One of the thermocouples was attached at 12 mm to 15 mm from the nozzle tip to measure temperature up to 780 °C in the center of the flame dome. The other thermocouple was attached at 22 mm from the nozzle tip to measure the substrate at around 550 °C. The flow rates of air and hydrogen were set to 7.87 L/min and 1.18 L/min, respectively.

Table 1. Parameters for the first experiment.

Sample #	Precursor Concentration mg/L	Atomizer Frequency MHz
1	50	3
2	100	3
3	200	3
4	50	2.4
5	100	2.4
6	200	2.4

The second set of experiments was conducted with the substrate preparation mentioned above with different concentrations (100 mg/L and 300 mg/L), and the temperature was adjusted around 780 °C at first, then increased to 830 °C.

3. Results and Discussion

In this section, the results of the experiments mentioned above are analyzed. The first experiment offered insight into the relation between nanoparticle size and experimental parameters, such as the concentration of precursor and the diameter of aerosol droplet. The second experiment shows the dependency of particle size on the flame temperature. Results of the third experiment verified that our system can produce one-step functional coatings. Silver nanoparticles are measured from scanning electron microscopy (SEM) images using image processing software, and the content was analyzed by EDX (Energy Dispersive X-ray).

3.1. Variable Concentration and Droplet Diameter

Silver nanoparticles were synthesized from the proposed nozzle design. The range of average particle size was from 25 nm to 40 nm with different experimental parameters. Table 2 summarizes the results to enumerate the average size and its standard deviation with different experiment sets.

Table 2. Average particle size with different conditions.

Sample #	1	2	3	4	5	6
Average size (nm)	40	37	33	28	27	25
Standard deviation (nm)	10.6	9.9	6.5	10.9	4.8	5.5

The results in Table 2 were counterintuitive because the largest nanoparticles were obtained from droplets with the smallest diameter at higher atomizer frequency, and lower concentration of the precursor resulted in larger average size of particles. Because all other parameters were kept constant for whole sets, the results were not caused by the different temperature of the droplets or their travel time over the flame dome.

A reason for the first tendency may be explained by the duration of the precursors to attain the temperature for thermal decomposition where nanoparticles begin to form. The time taken for larger droplets reaching the thermal decomposition temperature is delayed because an evaporative cooling effect occurs, and the thermal conductivity of water is relatively low since the precursor solution is based on water. In contrast, small droplets have a shorter time for thermal decomposition, such that the reaction begins earlier and continues for a longer time, and the droplets form larger nanoparticles and agglomerates with higher temperature than is the case for large droplets coalescing to solid particles [25]. Another possible explanation is that surface precipitation at low droplet concentration causes hollow pores, thereby increasing particle size. At high droplet concentration, volume precipitation generates denser and smaller particles [35]. Experiments to investigate the structure of nanoparticles are required in further research.

The second tendency that smaller nanoparticles are generated at higher precursor concentration can be explained by smaller droplets agglomerating to form larger clusters at lower precursor concentration, which is explained before since the sizes of the particles are small, larger agglomerates may be mistakenly considered as a single particle during SEM image analysis, which results in larger average size. It also explains larger standard deviations at lower concentration of the precursor.

Figure 4 illustrates the size distribution of the nanoparticles, which shows similar tendency to the other experiments. It is known that the size of nanoparticles is mostly governed by size of the precursor droplets by the atomizer. Since the size of droplets at the exit of the atomizer varies from 3 μm to 10 μm at 2.4 MHz resonant frequency of the atomizer, the nanoparticle size distribution can be more concentrated when the sizes of the precursor droplets are regularly distributed.

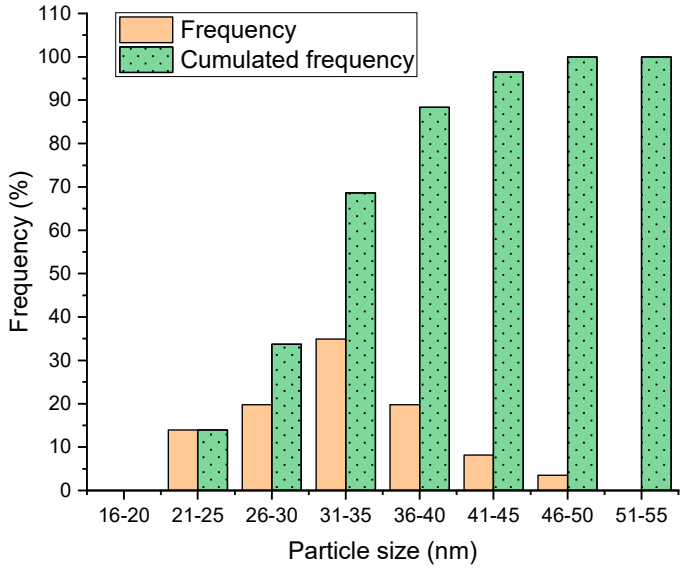

Figure 4. Size distribution of the nanoparticles for sample #3.

Figures 5 and 6 show SEM images of the resultant nanoparticles. The image was taken after depositing a layer of carbon for better charge dissipation. The specimen was analyzed in slow mode at 2 kV accelerating voltage with 45 K magnification and 1 kV with 100 K magnification. The image was captured at 5.1 mm working distance with 60% backscattering.

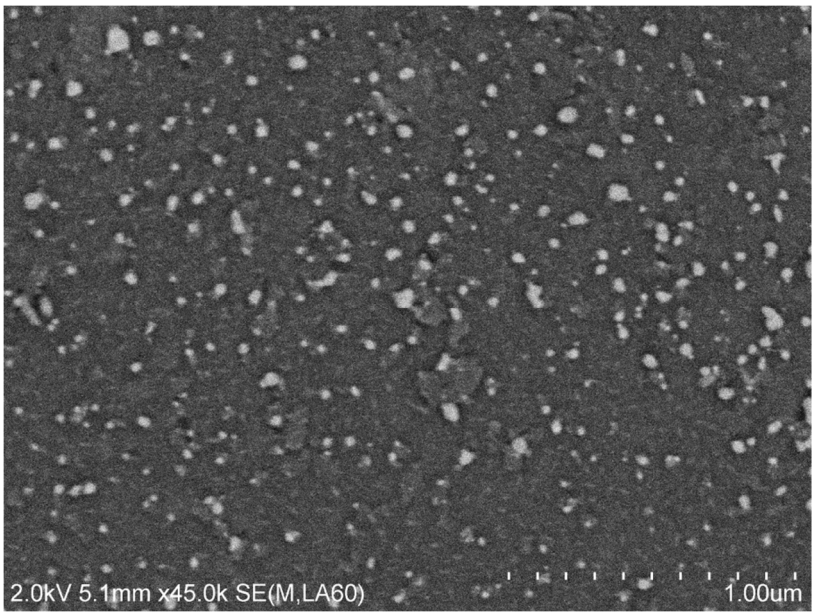

Figure 5. SEM image of sample #3 (concentration 200 mg/L, frequency 3 MHz).

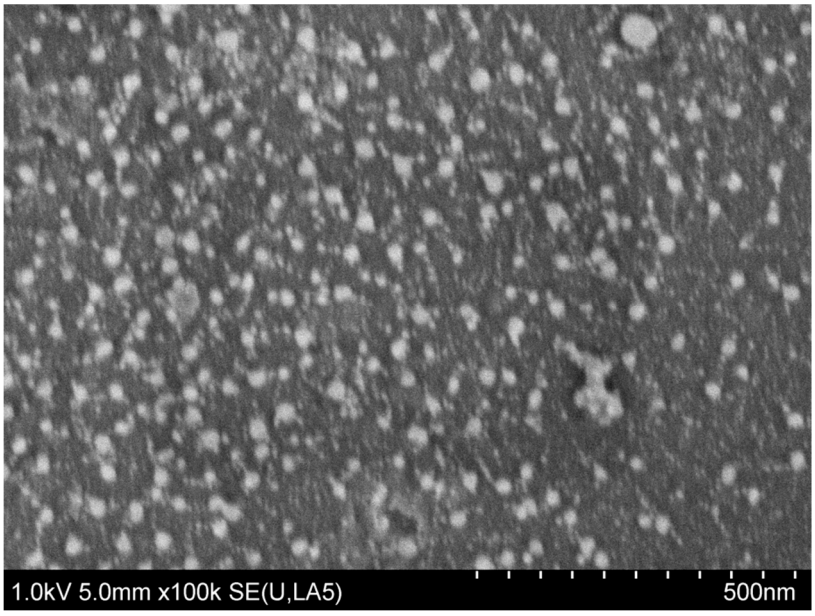

Figure 6. SEM image of sample #6 (concentration 200 mg/L, frequency 2.4 MHz).

Next, EDX (Energy Dispersive X-ray) analysis was performed using Bruker Quantex EDS system at 6 kV to investigate the spectrum of bright spots in the SEM images. The voltage was set to maximize the L-line emissions for silver. Having 2.983 kV potential and twice the amount of accelerating voltage maximizes emissions, which results in better imaging quality. The spectrum maps of sample #3 at 200,000× magnification in Figure 7 verify that the content of the nanoparticles is silver. In the EDX analysis, aluminum and nitrogen contents were also detected. Aluminum is from the substrate, but nitrogen content can be explained by some droplets reaching the substrate without

thermal decomposition and then drying on the surface. Figure 7 verifies that the clump of silver in the picture is not silver nitrate, since the clump is not visible in the picture of nitrogen. However, further measurements and analysis are needed to test for substances other than sliver, such as silver oxide (Ag_2O).

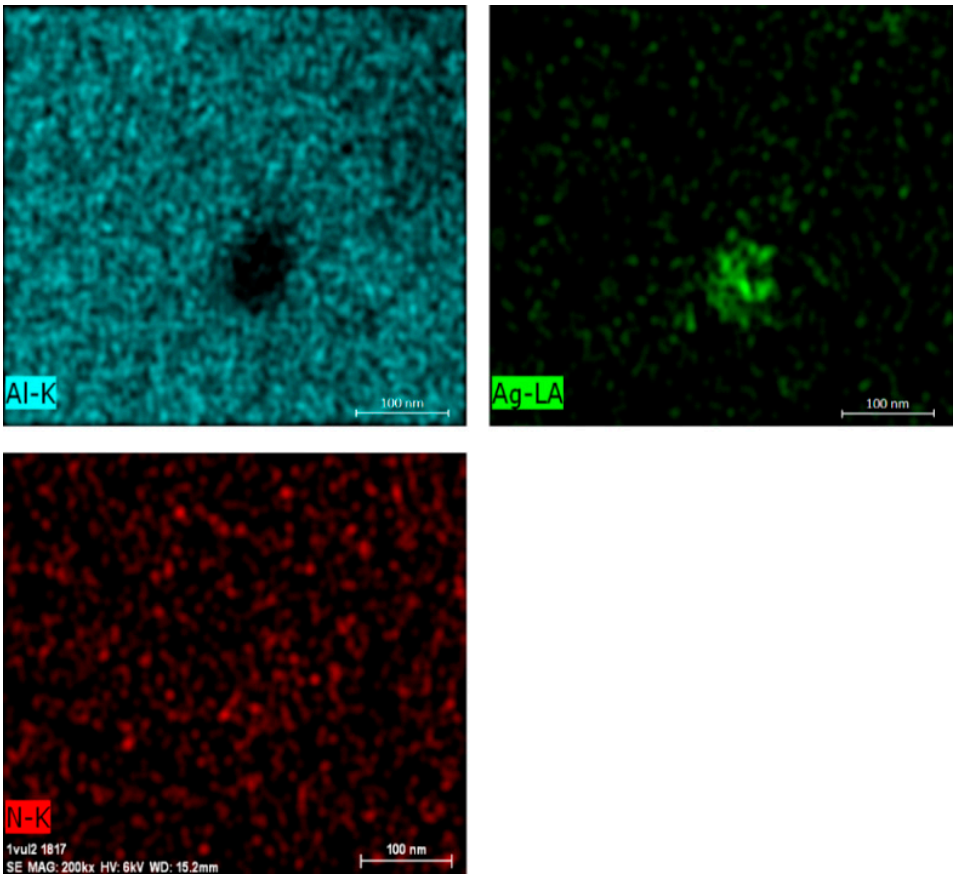

Figure 7. EDX analysis results of deposited nanoparticles.

3.2. Variable Flame Temperature

Table 3 summarizes the results of the second experiment. Samples #7 and #8 at lower flame temperature show a different tendency compared to the first experiment, demonstrating that nanoparticle size is increased at higher precursor concentration. However, nanoparticle size is drastically increased at higher flame temperature. These relationships agree with the other studies, however, Mäkela et al. [31] mentioned that the concentration of precursors has no effect to the nanoparticle size. The control of flame temperature seems to be more important for desired nanoparticle size distribution.

Table 3. Nanoparticle size with varying conditions.

Sample #	Flame Temperature (°C)	Precursor Concentration (mg/L)	Size of Nanoparticle (nm)
7	~780	300	35~60
8	~780	100	26~48
9	830	100	100~115

4. Conclusions

This paper proposes an annular nozzle design for flame-assisted spray pyrolysis to deposit nanoparticles. The nozzle with an ultrasonic nebulizer can control process parameters such as precursor

size, flame temperature, and the focus point of the jet. Effects of parameters such as the atomizer's natural frequency, precursor concentration, and flame temperature on the size of nanoparticles were studied. The ranges of the studied parameters were 50~300 mg/L precursor concentration, 2.4~3 MHz atomizer frequency, and 780~830 °C flame temperature, respectively. The first experiment showed that larger precursor droplets result in smaller nanoparticles, but less precursor concentration causes larger particle size due to agglomeration at high temperature. In the second experiment, increased flame temperature resulted in larger nanoparticle size, as described in previous studies. SEM and EDX analysis of the experiments verified that silver nanoparticles are deposited on aluminum substrates with the average size of 25~115 nm.

Further studies are required to improve the process. To reduce unwanted precursor residues, such as nitride and aluminum, fine tuning of process parameters such as precursor concentration, feed rate of the nozzle, flame temperature, and the distance between nozzle and substrate is required. In addition, the efficiency between consumed precursor and produced nanoparticles should be assessed, and further tuning of the parameters are required to improve the process.

Author Contributions: M.R. developed the nozzle spray system and wrote the paper. M.R. and S.B. performed experiments and analyzed the data. J.N., H.Y., and M.B.G.J. validated the results and proofread the manuscript. M.B.-G.J. guided the research.

Funding: The authors acknowledge the support of Korea Carbon Capture and Sequestration Research and Development Center (KCRC) and the Technology Innovation Program (10053248, Development of Manufacturing System for CFRP (Carbon Fiber Reinforced Plastics Machining) funded By the Ministry of Trade, industry & Energy (MOTIE, Korea) for this work.

Conflicts of Interest: The authors declare no conflict of interest.

References

1. Karthikeyan, J.; Berndt, C.; Tikkanen, J.; Wang, J.; King, A.; Herman, H. Nanomaterial powders and deposits prepared by flame spray processing of liquid precursors. *Nanostruct. Mater.* **1997**, *8*, 61–74. [CrossRef]
2. Mädler, L.; Roessler, A.; Pratsinis, S.E.; Sahm, T.; Gurlo, A.; Barsan, N.; Weimar, U. Direct formation of highly porous gas-sensing films by in situ thermophoretic deposition of flame-made Pt/SnO_2 nanoparticles. *Sens. Actuators B Chem.* **2006**, *114*, 283–295. [CrossRef]
3. Strobel, R.; Baiker, A.; Pratsinis, S.E. Aerosol flame synthesis of catalysts. *Adv. Powder Technol.* **2006**, *17*, 457–480. [CrossRef]
4. Rosner, D.E. Flame synthesis of valuable nanoparticles: Recent progress/current needs in areas of rate laws, population dynamics, and characterization. *Ind. Eng. Chem. Res.* **2005**, *44*, 6045–6055. [CrossRef]
5. Teisala, H.; Tuominen, M.; Aromaa, M.; Mäkelä, J.; Stepien, M.; Saarinen, J.; Toivakka, M.; Kuusipalo, J. Development of superhydrophobic coating on paperboard surface using the liquid flame spray. *Surface Coat. Technol.* **2010**, *205*, 436–445. [CrossRef]
6. Mäkelä, J.M.; Aromaa, M.; Teisala, H.; Tuominen, M.; Stepien, M.; Saarinen, J.J.; Toivakka, M.; Kuusipalo, J. Nanoparticle deposition from liquid flame spray onto moving roll-to-roll paperboard material. *Aerosol Sci. Technol.* **2011**, *45*, 827–837. [CrossRef]
7. Avvaru, B.; Patil, M.N.; Gogate, P.R.; Pandit, A.B. Ultrasonic atomization: Effect of liquid phase properties. *Ultrasonics* **2006**, *44*, 146–158. [CrossRef] [PubMed]
8. Hansen, J.P.; Jensen, J.R.; Livbjerg, H.; Johannessen, T. Synthesis of ZnO particles in a quench-cooled flame reactor. *AIChE J.* **2001**, *47*, 2413–2418. [CrossRef]
9. Johannessen, T.; Jensen, J.R.; Mosleh, M.; Johansen, J.; Quaade, U.; Livbjerg, H. Flame synthesis of nanoparticles: Applications in catalysis and product/process engineering. *Chem. Eng. Res. Des.* **2004**, *82*, 1444–1452. [CrossRef]
10. Jensen, J.R.; Johannessen, T.; Wedel, S.; Livbjerg, H. A study of $Cu/ZnO/Al_2O_3$ methanol catalysts prepared by flame combustion synthesis. *J. Catal.* **2003**, *218*, 67–77. [CrossRef]
11. Perednis, D.; Gauckler, L.J. Thin film deposition using spray pyrolysis. *J. Electroceram.* **2005**, *14*, 103–111. [CrossRef]

12. Pratsinis, S.E.; Zhu, W.; Vemury, S. The role of gas mixing in flame synthesis of Titania powders. *Powder Technol.* **1996**, *86*, 87–93. [CrossRef]
13. Mädler, L.; Kammler, H.; Mueller, R.; Pratsinis, S.E. Controlled synthesis of nanostructured particles by flame spray pyrolysis. *J. Aerosol Sci.* **2002**, *33*, 369–389. [CrossRef]
14. Mädler, L.; Stark, W.J.; Pratsinis, S.E. Flame-made ceria nanoparticles. *J. Mater. Res.* **2002**, *17*, 1356–1362. [CrossRef]
15. Kammler, H.K.; Mädler, L.; Pratsinis, S.E. Flame synthesis of nanoparticles. *Chem. Eng. Technol.* **2001**, *24*, 583–596. [CrossRef]
16. Pratsinis, S.E. Aerosol-based technologies in nanoscale manufacturing: From functional materials to devices through core chemical engineering. *AIChE J.* **2010**, *56*, 3028–3035. [CrossRef]
17. Tricoli, A.; Elmøe, T.D. Flame spray pyrolysis synthesis and aerosol deposition of nanoparticle films. *AIChE J.* **2012**, *58*, 3578–3588. [CrossRef]
18. Cho, K.; Chang, H.; Kil, D.S.; Park, J.; Jang, H.D.; Sohn, H.Y. Mechanisms of the formation of silica particles from precursors with different volatilities by flame spray pyrolysis. *Aerosol Sci. Technol.* **2009**, *43*, 911–920. [CrossRef]
19. Mäkelä, J.; Hellstén, S.; Silvonen, J.; Vippola, M.; Levänen, E.; Mäntylä, T. Collection of liquid flame spray generated TiO_2 nanoparticles on stainless steel surface. *Mater. Lett.* **2006**, *60*, 530–534. [CrossRef]
20. Aromaa, M.; Keskinen, H.; Mäkelä, J.M. The effect of process parameters on the liquid flame spray generated titania nanoparticles. *Biomol. Eng.* **2007**, *24*, 543–548. [CrossRef] [PubMed]
21. Guild, C.; Biswas, S.; Meng, Y.; Jafari, T.; Gaffney, A.M.; Suib, S.L. Perspectives of spray pyrolysis for facile synthesis of catalysts and thin films: An introduction and summary of recent directions. *Catal. Today* **2014**, *238*, 87–94. [CrossRef]
22. Pimenoff, J.; Hovinen, A.; Rajala, M. Nanostructured coatings by liquid flame spraying. *Thin Solid Films* **2009**, *517*, 3057–3060. [CrossRef]
23. Pratsinis, S.E. Flame aerosol synthesis of ceramic powders. *Prog. Energy Combust. Sci.* **1998**, *24*, 197–219. [CrossRef]
24. You, H.; Cho, K.; Yoon, Y.; Im, J.; Shin, D. Synthesis of yttria-stabilized zirconia film by Aerosol Flame Pyrolysis Deposition. *J. Anal. Appl. Pyrolysis* **2008**, *81*, 14–19. [CrossRef]
25. Mueller, R.; Mädler, L.; Pratsinis, S.E. Nanoparticle synthesis at high production rates by flame spray pyrolysis. *Chem. Eng. Sci.* **2003**, *58*, 1969–1976. [CrossRef]
26. Tikkanen, J.; Gross, K.; Berndt, C.; Pitkänen, V.; Keskinen, J.; Raghu, S.; Rajala, M.; Karthikeyan, J. Characteristics of the liquid flame spray process. *Surface Coat. Technol.* **1997**, *90*, 210–216. [CrossRef]
27. Teoh, W.Y.; Amal, R.; Mädler, L. Flame spray pyrolysis: An enabling technology for nanoparticles design and fabrication. *Nanoscale* **2010**, *2*, 1324–1347. [CrossRef] [PubMed]
28. Purwanto, A.; Widiyandari, H.; Jumari, A. Fabrication of high-performance fluorine doped–tin oxide film using flame-assisted spray deposition. *Thin Solid Films* **2012**, *520*, 2092–2095. [CrossRef]
29. Pluym, T.; Powell, Q.; Gurav, A.; Ward, T.; Kodas, T.; Wang, L.; Glicksman, H. Solid silver particle production by spray pyrolysis. *J. Aerosol Sci.* **1993**, *24*, 383–392. [CrossRef]
30. Pingali, K.C.; Rockstraw, D.A.; Deng, S. Silver nanoparticles from ultrasonic spray pyrolysis of aqueous silver nitrate. *Aerosol Sci. Technol.* **2005**, *39*, 1010–1014. [CrossRef]
31. Mäkelä, J.; Keskinen, H.; Forsblom, T.; Keskinen, J. Generation of metal and metal oxide nanoparticles by liquid flame spray process. *J. Mater. Sci.* **2004**, *39*, 2783–2788. [CrossRef]
32. Kim, D.; Jeong, S.; Moon, J. Synthesis of silver nanoparticles using the polyol process and the influence of precursor injection. *Nanotechnology* **2006**, *17*, 4019. [CrossRef] [PubMed]
33. Rukosuyev, M.V.; Barannyk, O.; Oshkai, P.; Jun, M.B. Design and application of nanoparticle coating system with decoupled spray generation and deposition control. *J. Coat. Technol. Res.* **2016**, *13*, 769–779. [CrossRef]

34. Jiang, C.; Nie, J.; Ma, G. A polymer/metal core–shell nanofiber membrane by electrospinning with an electric field, and its application for catalyst support. *RSC Adv.* **2016**, *6*, 22996–23007. [CrossRef]
35. Jokanović, V.; Spasić, A.M.; Uskoković, D. Designing of nanostructured hollow TiO_2 spheres obtained by ultrasonic spray pyrolysis. *J. Colloid Interface Sci.* **2004**, *278*, 342–352. [CrossRef] [PubMed]